

High Temperature Applicable Separator by Using Polyimide aerogel/polyethylene Double-Layer Composite Membrane for High-Safety Lithium Ion Battery

Gunhwi Kim[#], Jinyoung Kim[#], Jongyeob Jeong, Daero Lee, Myeongsoo Kim, Sangrae Lee, Seohyun Kim, Hyunju Lee, Haksoo Han*

Department of Chemical and Biomolecular Engineering, Yonsei University, 262 Seongsan-no, Seodaemun-gu, Seoul 120-749, South Korea

E-mail: hshanpublication@gmail.com

[#]These two authors have equally contributed to this study

Received: 5 March 2018 / Accepted: 16 July 2018 / Published: 30 June 2019

To address the vulnerability of a conventional separator to high temperature, a new double-layer function of separator with a double-layer function is suggested for high-safety lithium-ion batteries that are used in harsh condition. The new composite separator was fabricated by coating thermally imidized polyimide aerogel (PIA) on a porous polyethylene (PE) membrane, with polyvinylidene fluoride (PVDF) as a binder, to improve the thermal stability of the separator. The PIA/PE double-layer composite performed very well, especially in terms of thermal stability. The newly suggested separator showed a near-zero thermal shrinkage rate compared to commercial PE separators, which are defective in having high levels of the same, and retained its structure up to 140 °C. The PIA supporting layer showed hardly any change after heat treatment, and the PE layer performed its role as a shut-down layer perfectly, ensuring the safety of the new separator. These results prove that a PIA/PE separator can prevent batteries from exploding and overcharging. In addition, the PIA/PE separator also demonstrated excellent electrolyte uptake and electrolyte wettability to electrolyte. PIA/PE separator based coin cells exhibited outstanding cycling and rate performances, especially at high current rates, compared to coin cells with a standard PE separator. Therefore, the new PIA/PE separator is an ideal candidate for use in high-safety lithium-ion batteries at high temperatures, based on its excellent thermal and chemical stability.

Keywords: Polyimide aerogel; Separator; Composite; Lithium-ion battery; Safety; Thermal stability.

1. INTRODUCTION

Lithium ion batteries have recently been highly sought after and are used in various industries [1]. To keep up with the rapid developments in technology, high-performance lithium-ion batteries with higher capacities are in strong demands [1–4]. To achieve this, researchers demonstrated various approaches to thin the separator and invest more in the cathode and anode [5–7]. However, they neglected to improve safety thresholds to accommodate their efforts to amplify performance. The result was many accidents related to explosions of lithium batteries; these were important issues in 2016, and revealed the vital role of the separator in battery systems [8–10]. A separator works in a battery system as an electron pathway and as a partition between the cathode and anode, thus preventing failures due to short-circuits [11,12]; it is also considered the main suspected cause for explosions of the secondary cell. Polyethylene and polypropylene porous membranes are the polyolefin materials mostly commonly used as commercial separators [13,14]. Although porous membranes are good candidates for separators with great chemical stability and mechanical properties, their melting point ranges from 130 °C to 160 °C, which is too low to be applied in a high temperature environment. They also have several drawbacks, such as a low thermal stability, which sometimes leads to shrinkage occurring below the melting point, and a low liquid electrolyte wettability. Therefore, in special situations such as operation in hot environments or overheating caused by overcharging, their low thermal stability induces dimensional shrinkage [15–17]. In addition, the contraction of the separator can also cause contact between the cathode and anode, which leads to a dangerous explosion or a conflagration of the secondary cell system. Therefore, blocking its own pores to prevent such contact, and thus shutting down the operating system in such a situation, is a significant requirement of a separator [18–20].

Separators do not seriously affect electrical performance; however, they have a significant role in terms of safety. Firstly, a separator should be able to block its pores at high temperatures, without contracting, to halt electron transfer. In addition, high porosity, electrolyte wettability, and excellent electrolyte uptake are required in an efficient separator [21–24]. To satisfy these requirements, a polyimide aerogel/polyethylene (PIA/PE) separator was fabricated by coating PIA with a high porosity and good thermal stability on a PE membrane layer with polyvinylidene fluoride (PVDF) as a binder. When overcharged, the temperature reaches the melting point of PE (about 130 °C) and the membrane starts to shrink. PE melts completely, becomes colorless, and remains as a collapsed structure. In contrast, the PE layer of a PIA/PE separator melts and blocks its pores, while the PIA's high thermal stability of PIA prevents the shrinkage of the PIA/PE membrane.

Researchers have continuously tried to apply Polyimide (PI) to fabricate a secondary cell separator with a high thermal and chemical stability [25–27]. However, existing research on applying polyimide to the fabrication of separators produced separators mainly by dissolving chemically imidized PI powder and remolding it, to bypass the problem of the low thermal stability of the shutdown layer, which is incompatible with the thermal curing process of traditional PI. However, the fabricated PI layer in this study has a relatively lower porosity and can be re-dissolved easily [28–30]. Therefore, to improve these properties, the PIA used here was fabricated using thermal curing, mixed with the PVDF binder and was coated on the PE layer. These steps stabilized the double-layer

membrane. Repeated measurements, indicated that the newly developed separator showed excellent behavior in terms of thermal, chemical, and physical properties.

2. EXPERIMENTAL

2.1 Materials

For this study, pyromellitic dianhydride (PMDA) and 4,4'-oxydianiline (ODA), with purity > 98%, were bought from Tokyo Chemical Industry Co. Ltd (Tokyo, Japan). Anhydrous 1-methyl-2-pyrrolidinone (NMP) and with purity > 99% was purchased from Duksan Pure Chemicals Co. Ltd (Gyeonggi-Do, Korea). A bolt closure-type autoclave (Ilshin, Daejeon, Korea), capable of carrying out experiments up to 11.7MPa and 250°C, was used. PVDF was purchased from Sigma Aldrich (Darmstadt, Germany). LiPF₆ 1M EC/DEC (1:1 v/v), which was used as the electrolyte, was purchased from Soulbrain Co.Ltd (Seongnam, Korea). Polyethylene membrane (t16-518) was purchased from SK (Gyeonggi-Do, Korea).

2.2 Fabrication of polyimide aerogel

Poly (amic acid) solution, the precursor of polyimide, was prepared by reacting PMDA (2.18 g, 10 mmol) and ODA (2.0024 g, 10 mmol) with NMP (20 mL) as the solvent. ODA was first dissolved in NMP, and PMDA was then added to the solution to prepare the PAA solution. The PAA solution was synthesized by polymerizing of PMDA and ODA. It was then stirred for 24 h at room temperature (20 °C) under a nitrogen (N₂) atmosphere. This solution was the precursor of the polyimide aerogel.

The PAA solution was placed in the autoclave in 30 mL glass vial. The space between the glass vial and the autoclave was filled with acetone halfway up the height of the bottle, to create a high-pressure atmosphere in the autoclave during the curing process. The autoclave system was sealed airtight and put into a curing oven. The temperature profile of the curing process is set as follows: 180 °C at a ramp rate of 2 °C/min, maintained at 180 °C for 6 h, and cooled at a ramp rate of 2 °C/min. After the curing process, the glass bottle was put into a vacuum oven and dried under a vacuum at 80 °C for 24 h to completely remove residual solvent.

2.3 Preparation of composite separators

The composite separators were fabricated using a solution casting method. The PE separator was used as a coating substrate. Aerogel particles used as a supporting layer and the PVDF binder were prepared at a weight ratio of 9:1, and mixed with NMP. The resulting slurry was stirred in a clay pot for 30 min. The slurry was then coated onto one side of the porous PE separator using a doctor blade to ensure uniform thickness. We coated only one side of the PE membrane because it was enough to prevent the composite membrane from shrinking at a high temperature. The final product was dried under vacuum at 80 °C for 24 h to obtain the PIA/PE separator.

2.4 Electrode preparation and cell assembly

Lithium metal was used as the anode. The cathode was composed of 90 wt% LiCoO₂, 6 wt% Super-P, and 4 wt% PVDF. The NMP-based cathode slurry was coated on an aluminum foil and dried overnight in a vacuum oven at 80 °C. 2032-type coin cells were assembled by placing the anode–separator–cathode sequence in an Argon conditioned glovebox. An electrolyte solution was prepared containing 1 M LiPF₆ and a solvent mixture of ethylene carbonate (EC), dimethyl carbonate (DMC), (EC/DMC = 1/1 wt/wt, PuriEL, Soulbrain Co., Ltd., Korea).

2.5 Characterization of the separators

Field-emission scanning electron microscopy (FE-SEM, JEOL-7001F) was used to investigate the surface and cross-section's morphological characteristics. Images of the separator treated at a high temperature were also observed to verify its shut-down function. The membrane was frozen in liquid nitrogen and broken or cut to allow observations of the smooth cross-section images of the separators. A shrinkage test was implemented to confirm the shrinkage rate of each separator. The original PE separator and the composite separator were cut into 2 cm × 2 cm squares and sandwiched between two glass plates. Each membrane was treated at room temperature, 120 °C and 140 °C for 30min. The shrinkage rate of separator was then calculated according to the following equation:

$$\text{Shrinkage (\%)} = \frac{S_0 - S}{S_0} \times 100\%$$

where S₀ and S are the surface area of the separator before and after the heat-treating test, respectively. The static contact angle was measured to measure the wettability between the membrane and the electrolyte using a GSA-X contact angle measurement (Surface Technology Korea).

The quantity of electrolyte taken up can be an index of the electrochemical properties of a membrane. The solvent uptake of the separators was calculated according to the following equation:

$$\text{Uptake (\%)} = \frac{W - W_0}{W_0} \times 100\%$$

where W₀ is the weight of the separator before immersion, and W is the weight of the separator immersed in electrolyte.

To confirm the thermal stability of the separator, we measured the glass transition temperature (T_g) and thermal decomposition temperature (T_d) of each membrane. The T_g of each separator was measured using differential scanning calorimetry (DSC) with a ASTM D4065, at a scanning rate of 5 °C/min in the range of 0 °C~300 °C. The thermal decomposition temperature was measured by thermogravimetric analysis (TGA) with a Q50 instrument (TA Instruments, New Castle, DE, USA). Ionic conductivity was measured with an electrochemical impedance spectroscopy (IVIUM Technologies, Netherlands) and calculated according to the following equation:

$$\sigma = \frac{d}{R \times A}$$

where d is thickness of the separator, A is its effective area, and R is its resistance.

To observe the actual electrochemical behavior of cells using each separator, cycling performance tests and rate performance tests were conducted. For the charge–discharge test, the C-rate discharge capability of the cells was examined using a 16-channel automatic battery cycler (WBCS

3000, WonAtech). The cycling performance of cells using each separator was tested at 3.0 V~4.3 V at a constant current density of 0.5 C. The rate performance of each cell was evaluated at current rates of 0.2 C, 0.5 C, 1.0 C, 2.0 C, 3.0 C and 5.0 C

3. RESULT AND DISCUSSION

3.1. Characterization of polyimide aerogel

Several advantages can be expected when PIA is chosen as the supporting material for a separator, due to its superior characteristics such as a highly uniform porous structure, excellent thermal stability, and chemical stability. The PIA used in this study has a highly porous structure; this not only contributes to the improvement of electrolyte uptake rate, but also enhances the thermal stability. To investigate its microscopic morphology, the structure of the surface and interior of the PIA was observed using FE-SEM, and the images are shown in figure 1. From figures 1a and 1b, we observe that PIA particles are porous spheres with a uniform size of 5-6 μm . In figure 1c, a high resolution image of PIA is shown and its broccoli-like surface and numerous distributed nano-sized pores can be seen.

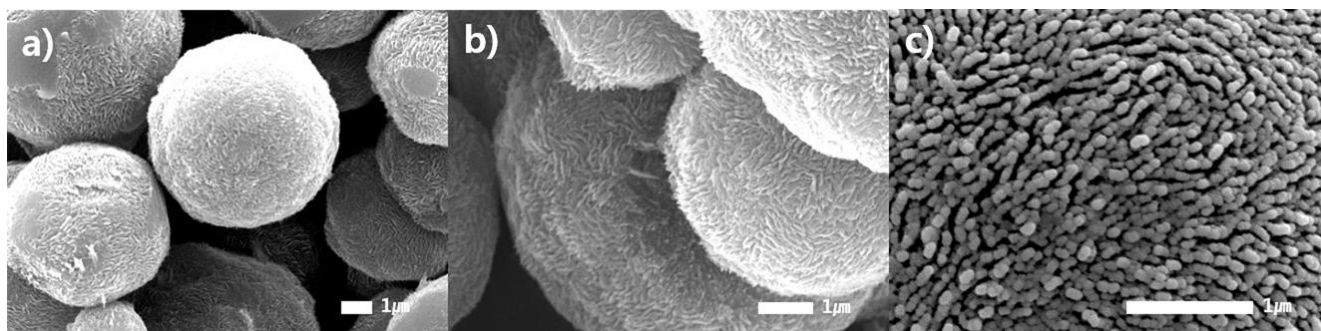


Figure 1. Field-emission scanning electron microscopy images of polyimide aerogel

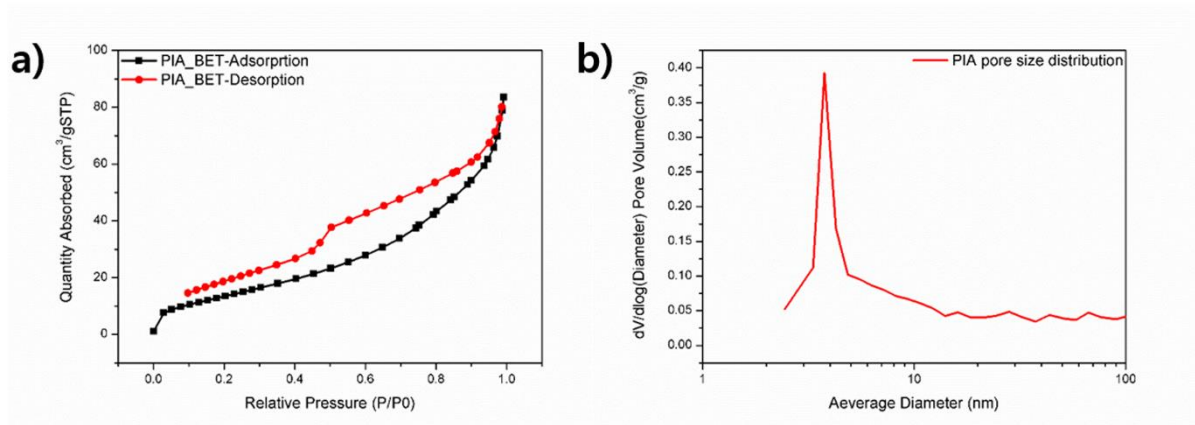


Figure 2. BET data of PIA. (a) adsorption and desorption curve of PIA, (b) pore size distribution of PIA

To verify its pore size distribution and porosity, PIA was measured using the Brunauer–Emmett–Teller method, and the results are shown in figure 2. The adsorption / desorption graph in figure 2a shows that many nano-sized pores formed in the PIA. Figure 2b shows that most of the pores are 3-4 nm in size. PIA was measured to have a high porosity of near 60%.

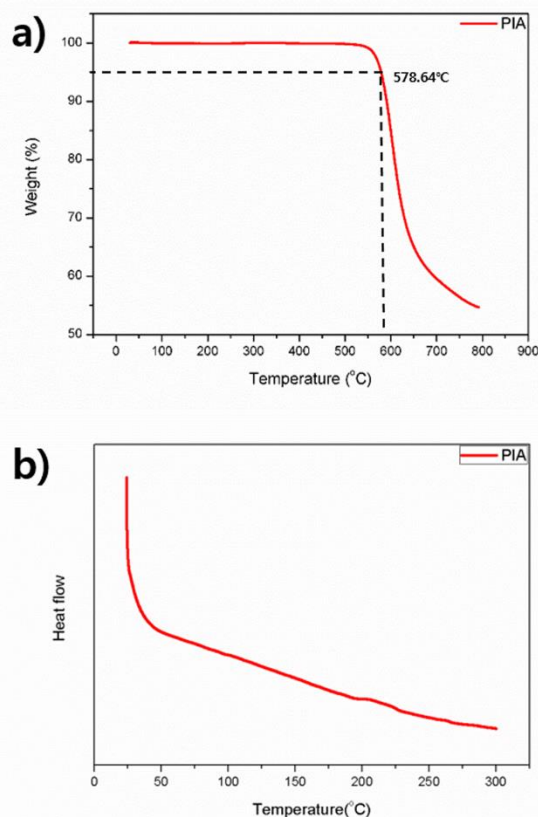


Figure 3. Thermal characteristics of PIA. (a) TGA curve of PIA, (b) DSC curve of PIA

We also confirmed the thermal stability of PIA using TGA and DSC; the results are shown in figure 3. Figure 3a shows that the 5% thermal decomposition temperature of the PIA, as measured by TGA is 578.64 °C; in figure 3b, the glass transition temperature of PIA is shown to be above 300 °C. Both the TGA and DSC data reveal that the thermal stability of the PI is maintained even after the structure is transformed to that of a spherical aerogel shape.

In general, PI is well known as a chemically stable material, there are two types of PI, thermally imidized and chemically imidized, that vary according to the different curing process used: The former is the mostly commonly utilized type of PI.. However, it is difficult to shape because of its insolubility to organic/inorganic solvents, which is why chemically imidized PI was invented by adding a functional group that has an affinity with organic solvents. It is well known that thermally cured polyimide has higher chemical stability compared to chemically imidized polyimide, to choose the more stable one, both chemically imidized and thermally cured PI film were soaked in an organic solvent (dimethylacetamide), and their results are shown in figure 4. The chemically imidized film, which was dissolved in the organic solvent and then re-molded, dissolves quickly again in the solvent.

In comparison, the PI film cured at above 200 °C maintained its structure. Most studies on secondary cells use chemically imidized PI as a base material. However, because it is easily dissolved in the organic solvent, using thermally cured PI is much more suitable in battery fields. For these reasons, we selected thermally cured PIA as the supporting material in this work.

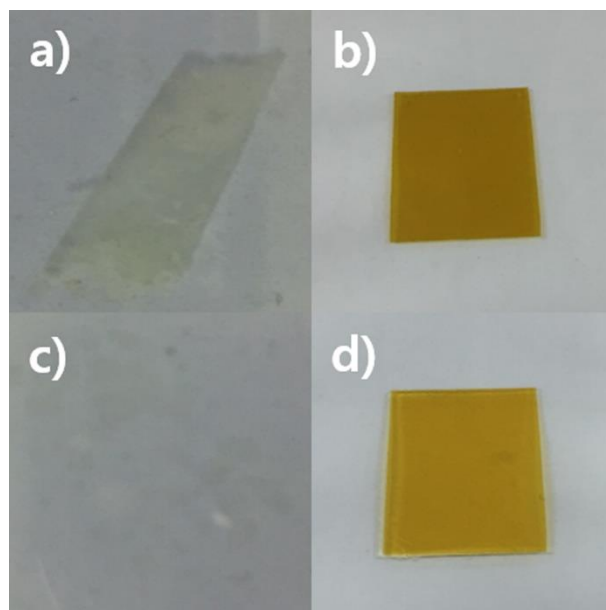


Figure 4. Photographs of chemically imidized polyimide (a) before and (c) after being immersed in organic solvent, and Images of thermally imidized polyimide (b) before and (d) after being immersed in organic solvent

3.2 Morphological property analysis of the PIA/PE separator

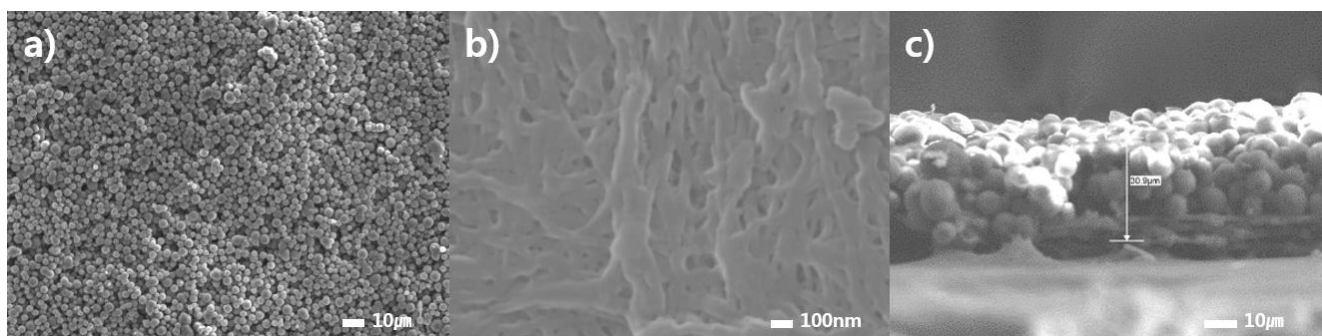


Figure 5. Field-emission scanning electron microscopy FE-SEM images of a polyimide aerogel/polyethylene PIA/PE separator before heat treatment: (a) Top surface of PIA/PE, (b) bottom surface of PIA/PE, (c) cross-section of PIA/PE

To observe the morphological structure of the PIA/PE separator, the sample was tested using FE-SEM, and the results are shown in figure 5. Figures 5a and 5b are the front and back surface images respectively. The front surface image shows that PIA is well dispersed and coated on the PE film without any aggregation. The back surface of the PE layer showed random pores.

The cross-sections of the film were measured using FE-SEM after cutting in liquid nitrogen. In figure 5c, the coated PIA shows a uniform thickness. Two layers were obviously well separated, the PE layer was completely covered by PIA layer. The height of the PE layer is $\sim 10\ \mu\text{m}$ and that of the PIA layer is $\sim 20\ \mu\text{m}$, therefore the total height of the film is $\sim 30\ \mu\text{m}$. This composite film was constructed compactly covered with polyimide based aerogel which has well distributed nano-size pores. The binder solution made of PVDF does not affect the porous structure of PIA which retained its original porous shape to maintain its great electrolyte uptake ability.

3.3 Thermal properties of the PIA/PE separator

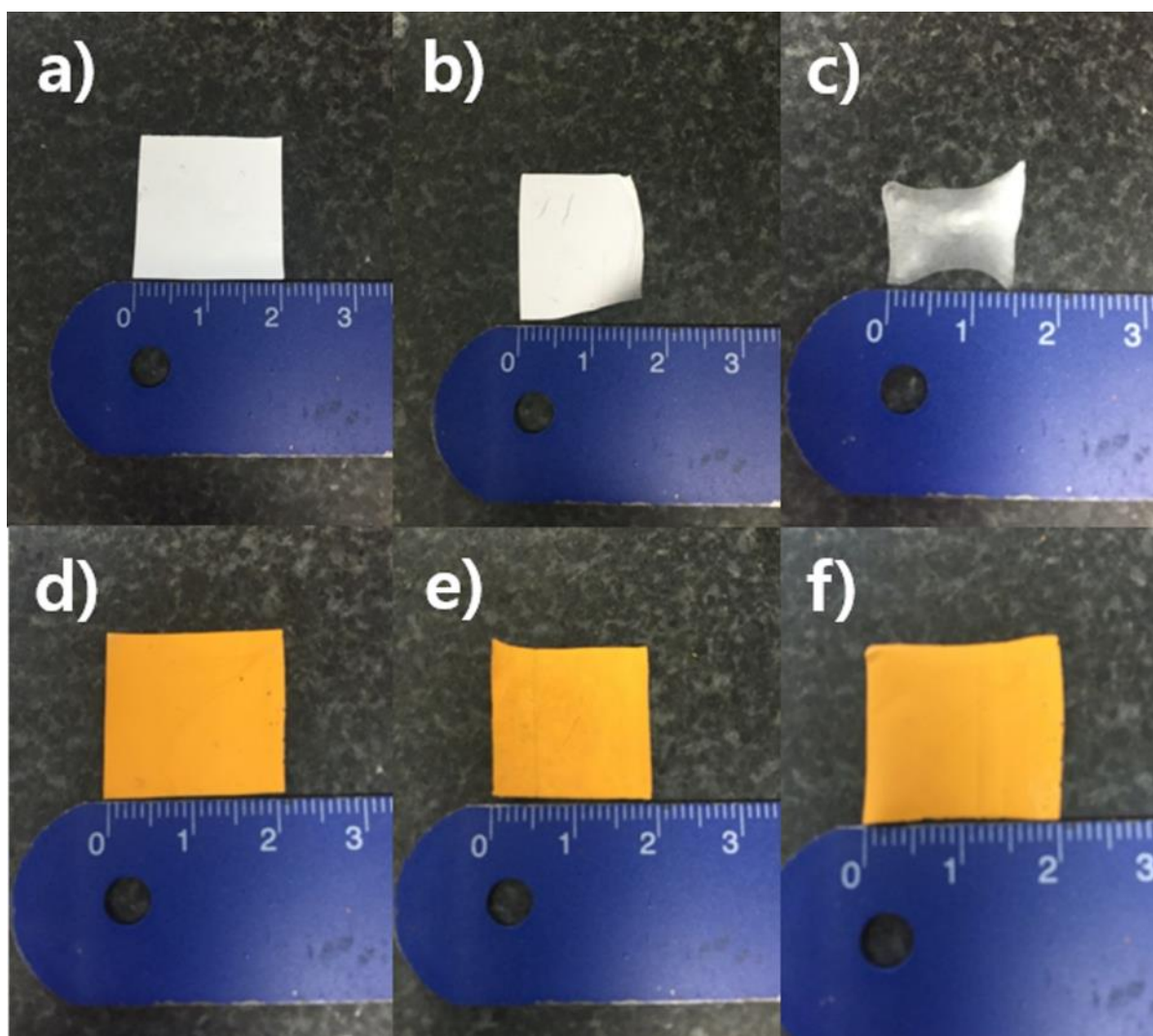


Figure 6. Photographs of PE separator and PIA separator (a) (d) before and (b) (e) being held in 110 °C for 30 min, (c) (f) 140 °C for 30 min

The Separator plays a significant role in the secondary cell as a division between the cathode and the anode. Therefore, the most important property required for a separator is low thermal shrinkage which can prevent a short circuit from occurring due to contact between the cathode and

anode in an overheated secondary cell. During the cycle, the separator should maintain its structure against the heat generated. However commercial separators are composed mainly of PE and polypropylene (PP), which have melting points of 130 °C and 160 °C respectively, this need to be improved. They shrink rapidly at temperatures above 130 °C and thus lose their ability to prevent contact between the cathode and the anode. Therefore, the low stability of commercial separators causes serious problems such as the explosion of the secondary cell. To prevent these issues, the thermal shrinkage rates of the newly fabricated PIA/PE separator were tested and compared with that of a commonly used PE separator. Each was cut into a specific size and heated at 110 °C, and 140 °C for 30 minutes, the resulting dimensional changes are shown in figure 6. During the thermal treatment, the separator was placed between two glass plates to simulate the condition of a secondary cell and prevent asymmetric warping on one side. Figure 6a and 6d show the original samples, were cut into 2 cm× 2 cm pieces. As shown in figures 6b and 6e, after 30 min of heat treatment at 110 °C, the PE showed a shrinkage rate of above 10% even though the temperature was lower than its melting point. In contrast, the PIA/PE separator retained its original size, showing a 0% thermal shrinkage rate. To investigate the shrinkage rate in an overheated condition, we heated both the PE and PIA/PE separators up to 140 °C. These thermally treated samples are shown in figures 6c and 6f, the PE film melts, shows a shrinkage rate of 50% and loses its ability to act as a separator. In comparison, the PIA/PE separator showed a 0% shrinkage rate. According to the thermal shrinkage test, the PIA/PE separator showed excellent improvement in thermal stability, the PIA filler in the PIA/PE separator successfully the thermal shrinkage by adhering to the original film structure without any wrinkles occurring. There are also several studies on highly stable separators in secondary cells. For example, a TiO₂-PMMA coating on a microporous PE membrane also showed improved stability, exhibiting a decreased thermal shrinkage of about 29.6% at 140 °C; however, the newly demonstrated composite separator showed 0% shrinkage even at 140 °C [31]. Overall data and results of the comparison show a great improvement in the newly synthesized composite separator, since it can successfully block contact between the cathode and anode even at high temperatures. There are many kinds of separators are being studied and developed recently, and the following table shows the comparison of the thermal shrinkage data among those researches.

Table 1. Thermal shrinkage comparison between separator materials developed in researches recently.

Separator	Thickness (μm)	Thermal shrinkage (%) under 140 °C	Ref.
Bare PP	25	70%	[13]
Bare PE	10	50%	-
PAM-grafted PP	26	35%	[32]
TiO ₂ -PMMA	25	29.6%	[31]
PVDF/PET/HFP composite	23	Less than 10%	[33]
PIA/PE composite	29	Near 0%	-

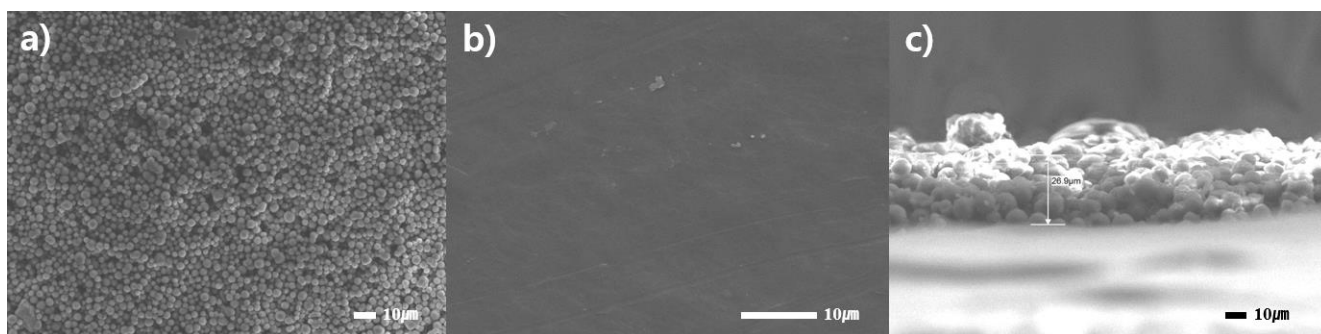


Figure 7. Field-emission scanning electron microscopy FE-SEM images of a polyimide aerogel/polyethylene PIA/PE separator after heat treatment in at 140 °C for 30 min: (a) Top surface of PIA/PE, (b) bottom surface of PIA/PE, (c) cross-section of PIA/PE

A microscopic investigation was conducted to verify the stable structure of the thermally treated PIA/PE separators. Figure 7, shows the morphology of the PIA/PE separator heat treated at 140 °C. According to figure 7a, the front surface of the PIA/PE separator, the PIA-coated side showed no change and maintained its structure without any aggregation or creases. Figure 7b, shows the back surface of the separator, which is the PE layer. In this FE-SEM image the PE layer melted and blocked all pores after 30 min of heat treatment at 140 °C. This indicates that it can completely stop the electric flows, demonstrating its great shut down ability. Both the significant requirements of a separator, which are a low dimensional change and an ability to shut-down were preserved successfully. In a previous thermal shrinkage test, the PIA/PE separator did not show any dimensional change and its highly porous structure was totally blocked by the melted PE membrane, which proved again that it meets both these essential requirements for a separator. Therefore, the PIA/PE film can be a great material with which to create the stable separator since it blocks electron pathways during harsh conditions that leads to heat being generated continuously in secondary cell, this would otherwise lead to dangerous conditions.

In figure 7c, an approximately ~27 μm cross-section of the film shows that only the PE layer melts down; the PIA layer maintained its structure. The commercial PE shows a dimensional change near its melting point, but the PIA/PE separator shows that only the melted PE enters the pores and that the height of the film changed without the occurrence of any dimensional changes which in turn could prevent contact between the cathode and the anode.

Figure 8 shows the DSC curves plotted to verify the thermal stability of the separator according to its glass transition temperature. In figure 8a, T_g is measured in 137 °C in figure 8b. As expected, since the PIA/PE film is fabricated by coating the surface of the PE film with PIA, the heat flow showed a critical change at 135 °C the T_g of PE. We confirmed the thermal stability of PIA using the TGA data in figures 8c, and 8d, in the former the PE membrane showed 10% thermal decomposition at a temperature of about 459.05 °C, while in the latter, the T_d of PIA is around 570 °C. Based on this result of the thermal shrinkage test, we verified that the PIA used herein, with its high thermal stability, has great potential as an ideal coating material for A separator to prevent short circuits in battery systems.

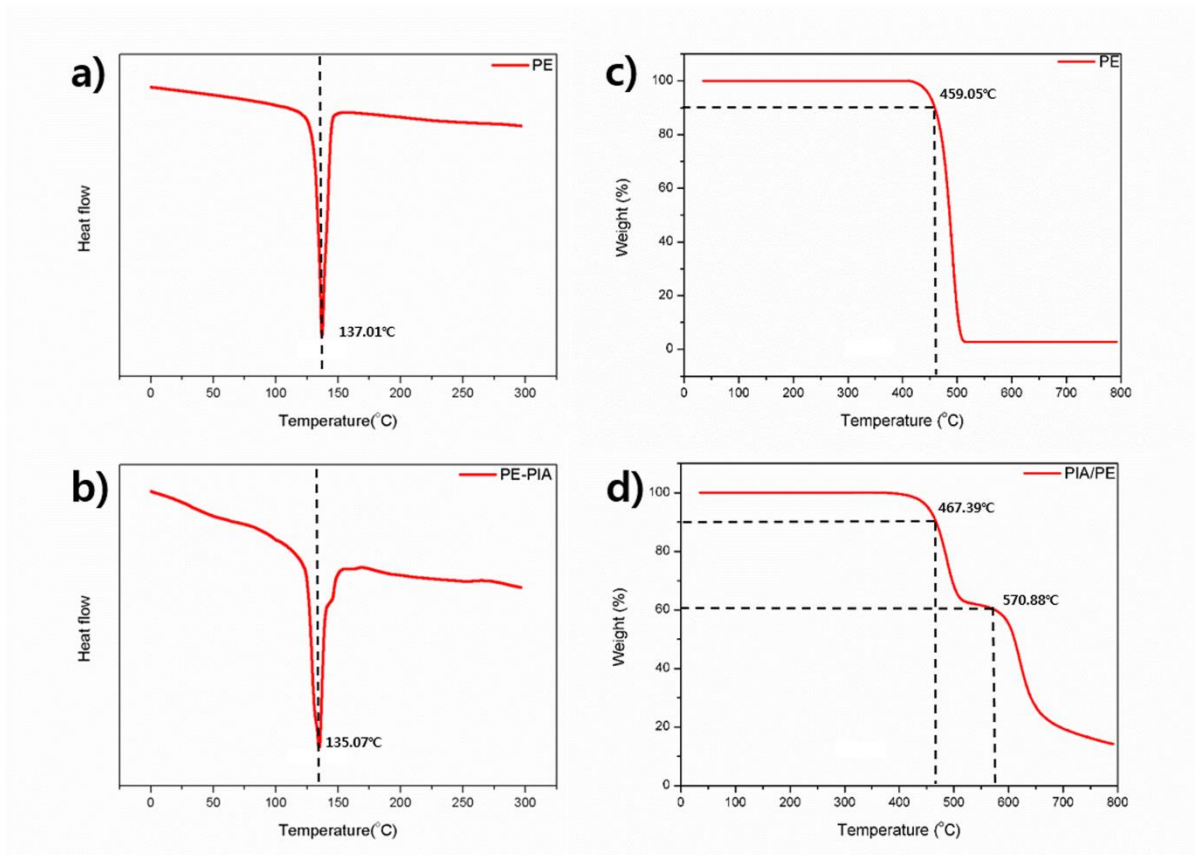


Figure 8. DSC curves of (a) PE, (b) PIA/PE and TGA curves of (c) PE, (d) PIA/PE

3.4 Wettability of separator to electrolyte and its electrochemical properties

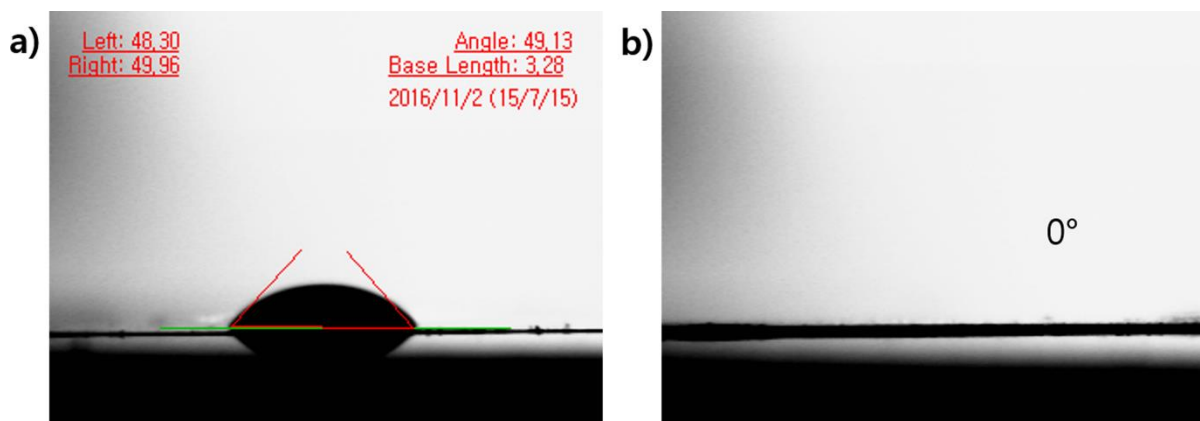


Figure 9. Wettability of the separator toward the electrolyte. (a) Contact angle of PE, (b) contact angle of PIA/PE

The electrolyte wettability of a separator is also a significant property that has a highly influences on the efficiency of the cell. A separator with a high wettability stimulates the lithium-ion

transfer in the secondary lithium cell. The contact angle was measured to determine the electrolyte wettability of the separator and the result is shown in figure 9. The contact angle is measured by dropping electrolyte solution onto the fixed separator. The PE separator had a contact angle of 49° to electrolyte, indicating that PE has a low electrolyte wettability. In contrast, the PIA/PE separator showed such an excellent wettability that it was not even possible to measure its exact contact angle, since it absorbed the electrolyte solution in a few second and shows as 0° in the data sheet. This shows that PI materials have a great affinity to electrolytes due to its carbonyl groups in chemical structure of PI[34,35], and that the high porosity of PIA about 80% also contributes to its high wettability[36,37].

An electrolyte uptake test was conducted to obtain the exact measurement of electrolyte contained in the separator. High electrolyte uptake directly influences the performance of the cell. The PE and PIA/PE separator were cut into pieces of the same size and soaked in electrolyte solution, and the weight difference was measured after 12 h. For accuracy, several tests were conducted and their average weight change was calculated.

According to table 1, the electrolyte uptake of the PE separator was 136.5%, and that of the PIA/PE was about 254%, which increased about two times. The porous structure of PIA on PE film can rapidly store great amount of electrolyte by capillary effect of well-connected nano-sized pores, which improves the electrolyte uptake of the separator[38,39].

Table 2. Electrolyte uptake and ionic conductivity data of PE and PIA/PE separators.

Separator	PE separator	PIA/PE separator
Average electrolyte uptake (g)	0.017	0.0623
Average electrolyte uptake (%)	136.5	254
Ion conductivity (mS/cm)	0.76	0.46

The PE separator measured 0.76 mS/cm in ionic conductivity measurements, but the PIA/PE separator had a value of 0.46 mS/cm. The thickness of the coating layer may be the main reason for this decrease, since a higher ionic conductivity can be expected if the coating layer is thinner, and the electrolyte uptake of the PIA/PE separator exceeded that of the PE separator remarkably.

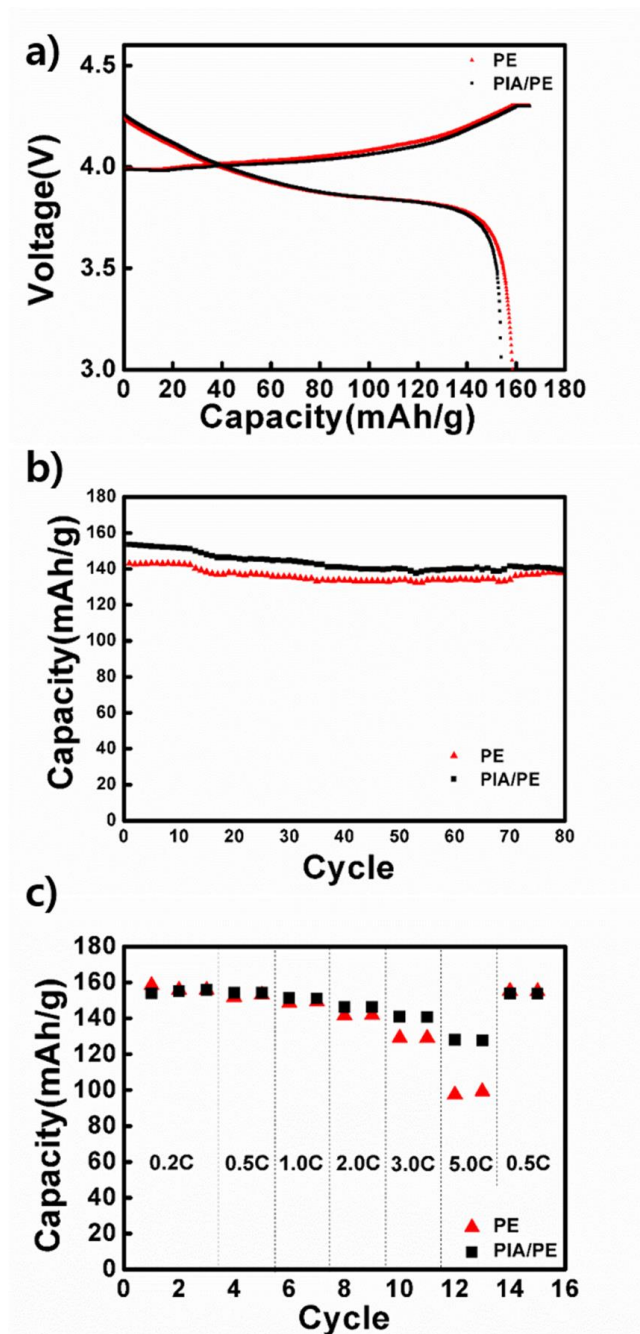


Figure 10. Electrochemical characteristic of coin cells with PE separator and PIA/PE separator. (a) Initial voltage profiles at 0.2 C, (b) rate performance of cells with PE and PIA/PE, (c) cycling performance of cells with PE and PIA/PE

The influence of the coated aerogel on the electrical performance was measured by constructing Li/LiCoO₂ coin-type half cells with potential ranging from 3.0 V-4.3 V at 0.2 C, and the final data are plotted in figure 10. Figure 10a shows the result of the first charge-discharge profile by using both the PE separator and the PIA/PE separator in which the data of each separators. There was no noticeable difference in data for each separator.

The cycling performance of PE and PIA/PE separators at 0.5 C at up to 80 cycles is shown in figure 10b. The latter showed higher initial discharge capacity of discharge than the former did.

Moreover, there is no difference in the capacity profiles of the two kinds of separator during the cycle. We can confirm that the PIA coating does not affect the electrochemical behavior of the batteries and that the PIA/PE separator showed a cycling stability similar to that of the PE separator.

The rate cell performance of two systems based on the PIA/PE and PE separators, respectively, is shown in figure 10c. The test range is 3.0 V-4.3 V for 0.2 C, 0.5 C, 1.0 C, 2.0 C, 3.0 C, and 5.0 C. There was no difference between two systems in the lower C-rate. However, since the current rate was set higher than this value, the capacity decreased. According to the plot, the capacity of PE-based cells showed a rapid tendency in reduction, compared to the gradual decrease rate of the one based on the PIA/PE separator. The high C-rate was rated an excellent performance, especially for about 5.0 C. The PIA/PE separator cell showed an excellent rate performance based on the high electrolyte uptake and high wettability of the separator which stimulated the lithium-ion mobility and the excellent retaining ability of the electrolyte.

4. CONCLUSION

A PIA/PE double layer composite membrane for use in a battery separator at high temperature was successfully fabricated by coating a high porosity polyimide aerogel as the supporting layer onto one side of the PE membrane using PVDF as a binder. When the thermally imidized polyimide aerogel with a porosity approaching 60% is applied in the separator as a supporting layer, it has more stability in an organic solvent than the polyimide synthesized using chemical imidization. FE-SEM images of each separator before and after heat treatments show that PIA successfully supports the layer and reinforced the thermal stability of the whole composite membrane when increasing the temperature to 140 °C. Only the PE layer melted after this treatment and blocked pores so it could successfully stop the battery operation and prevent further increase of temperature of the system. Additionally, the PIA/PE separator showed 0% thermal shrinkage compared to the use of the PE separator alone. Using the results of electrolyte uptake and contact angle test, we can confirm that PIA/PE's wettability is highly enhanced based on the PIA supporting layer. Although there are some drawbacks to the ionic conductivity of the PIA/PE and cycling performance, it shows a similar cycling performance as the original PE membrane in the first cycle. However, the PIA/PE composite separator shows outstanding rate performance especially at high current rate which is much higher than that of the PE separator. The properties and performance data of PIA/PE separator show that it can be an ideal separator for achieving high battery performances with increased cell safety.

ACKNOWLEDGEMENTS

This research was supported by Basic Science Research Program through the National Research Foundation of Korea(NRF) funded by the Ministry of Education(2017R1D1A1B03033332). This research was also supported by the Human Resources Program in Energy Technology of the Korea Institute of Energy Technology Evaluation and Planning (KETEP), granted financial resource from the Ministry of Trade, Industry & Energy, Republic of Korea. (No. 20174010201640)

References

1. H. Abe, M. Kubota, M. Nemoto, Y. Masuda, Y. Tanaka, H. Munakata, K. Kanamura, *J. Power Sources*. 334 (2016) 78–85.
2. S. Huang, B.E. Wilson, W.H. Smyrl, D.G. Truhlar, A. Stein, *Chem. Mater.* 28 (2016) 746–755.
3. S.J. Kim, M. Naguib, M. Zhao, C. Zhang, H.T. Jung, M.W. Barsoum, Y. Gogotsi, *Electrochim. Acta*. 163 (2015) 246–251.
4. S. Li, J. Niu, Y.C. Zhao, K.P. So, C.A.C.C.A.C. Wang, C.A.C.C.A.C. Wang, J. Li, *Nat. Commun.* 6 (2015) 7872.
5. J.M. Whiteley, P. Taynton, W. Zhang, S.H. Lee, *Adv. Mater.* 27 (2015) 6922–6927.
6. K. Park, J.H. Cho, K. Shanmuganathan, J. Song, J. Peng, M. Gobet, S. Greenbaum, C.J. Ellison, J.B. Goodenough, *J. Power Sources*. 263 (2014) 52–58.
7. S.M. Seidel, S. Jeschke, P. Vettikuzha, H.-D. Wiemhöfer, *Chem. Commun.* 51 (2015) 12048–12051.
8. J. Shi, Y. Xia, Z. Yuan, H. Hu, X. Li, H. Zhang, Z. Liu, *Sci. Rep.* 5 (2015) 8255.
9. J. Zhang, L. Yue, Q. Kong, Z. Liu, X. Zhou, C. Zhang, Q. Xu, B. Zhang, G. Ding, B. Qin, Y. Duan, Q. Wang, J. Yao, G. Cui, L. Chen, *Sci. Rep.* 4 (2014) 3935.
10. H. Wu, D. Zhuo, D. Kong, Y. Cui, *Nat. Commun.* 5 (2014) 5193.
11. H.S. Jeong, D.W. Kim, Y.U. Jeong, S.Y. Lee, *J. Power Sources*. 195 (2010) 6116–6121.
12. K.W. Song, C.K. Kim, *J. Memb. Sci.* 352 (2010) 239–246.
13. X. Huang, J. Hitt, *J. Memb. Sci.* 425–426 (2013) 163–168.
14. H. Li, Z. Wang, L. Chen, X. Huang, *Adv. Mater.* 21 (2009) 4593–4607.
15. Y. Zhang, Z. Wang, H. Xiang, P. Shi, H. Wang, *J. Memb. Sci.* 509 (2016) 19–26.
16. J.A. Choi, S.H. Kim, D.W. Kim, *J. Power Sources*. 195 (2010) 6192–6196.
17. K.J. Kim, J.H. Kim, M.S. Park, H.K. Kwon, H. Kim, Y.J. Kim, *J. Power Sources*. 198 (2012) 298–302.
18. M. Xiong, H. Tang, Y. Wang, M. Pan, *Carbohydr. Polym.* 101 (2014) 1140–1146.
19. M.Y. An, H.T. Kim, D.R. Chang, *J. Solid State Electrochem.* 18 (2014) 1807–1814.
20. Y. Liu, H. Ma, B.S. Hsiao, B. Chu, A.H. Tsou, *Polym. (United Kingdom)*. 107 (2016) 163–169.
21. X. Zhu, X. Jiang, X. Ai, H. Yang, Y. Cao, *ACS Appl. Mater. Interfaces*. 7 (2015) 24119–24126.
22. R. Darling, K. Gallagher, W. Xie, L. Su, F. Brushett, *J. Electrochem. Soc.* 163 (2016) A5029–A5040.
23. Z. Wang, H. Xiang, L. Wang, R. Xia, S. Nie, C. Chen, H. Wang, *J. Memb. Sci.* 553 (2018) 10–16.
24. C. Shi, J. Zhu, X. Shen, F. Chen, F. Ning, H. Zhang, Y.-Z. Long, X. Ning, J. Zhao, *RSC Adv.* 8 (2018) 4072–4077.
25. Y. Wang, S. Wang, J. Fang, L.-X. Ding, H. Wang, *J. Memb. Sci.* 537 (2017) 248–254.
26. L. Kong, L. Yuan, B. Liu, G. Tian, S. Qi, D. Wu, *J. Electrochem. Soc.* 164 (2017) A1328–A1332.
27. J. Hou, W. Jang, S. Kim, J.-H. Kim, H. Byun, *RSC Adv.* 8 (2018) 14958–14966.
28. D. Wu, C. Shi, S. Huang, X. Qiu, H. Wang, Z. Zhan, P. Zhang, J. Zhao, D. Sun, L. Lin, *Electrochim. Acta*. 176 (2015) 727–734.
29. C. Shi, P. Zhang, S. Huang, X. He, P. Yang, D. Wu, D. Sun, J. Zhao, *J. Power Sources*. 298 (2015) 158–165.
30. C. Shi, J. Dai, X. Shen, L. Peng, C. Li, X. Wang, P. Zhang, J. Zhao, *J. Memb. Sci.* 517 (2016) 91–99.
31. Y. Xi, P. Zhang, H. Zhang, Z. Wan, W. Tu, H. Tang, *Int. J. Electrochem. Sci.* 12 (2017) 5421–5430.
32. M. Liu, P. Zhang, L. Gou, Z. Hou, B. Huang, *Mater. Lett.* 208 (2017) 98–101.
33. Y.S. Wu, C.C. Yang, S.P. Luo, Y.L. Chen, C.N. Wei, S.J. Lue, *Int. J. Hydrogen Energy*. 42 (2017) 6862–6875.

34. J.-H. Park, W. Park, J.H. Kim, D. Ryoo, H.S. Kim, Y.U. Jeong, D.-W. Kim, S.-Y. Lee, *J. Power Sources*. 196 (2011) 7035–7038.
35. J.-Y. Sohn, J.-S. Im, J. Shin, Y.-C. Nho, *J. Solid State Electrochem.* 16 (2012) 551–556.
36. P. Yang, P. Zhang, C. Shi, L. Chen, J. Dai, J. Zhao, *J. Memb. Sci.* 474 (2015) 148–155.
37. J.-H. Park, J.-H. Cho, W. Park, D. Ryoo, S.-J. Yoon, J.H. Kim, Y.U. Jeong, S.-Y. Lee, *J. Power Sources*. 195 (2010) 8306–8310.
38. W.-K. Shin, D.-W. Kim, *J. Power Sources*. 226 (2013) 54–60.
39. P. Arora, Z. Zhang, *Chem. Rev.* 104 (2004) 4419–4462.

© 2019 The Authors. Published by ESG (www.electrochemsci.org). This article is an open access article distributed under the terms and conditions of the Creative Commons Attribution license (<http://creativecommons.org/licenses/by/4.0/>).